frontiers | Frontiers in Earth Science

ORIGINAL RESEARCH
published: 03 June 2022
doi: 10.3389/feart.2022.916905

Late Pleistocene Slip Rates on an Active Normal Fault in the Northwestern Ordos Block, China

Xingwang Liu[1,2]*, *Zemin Gao*[3], *Yanxiu Shao*[4] and *Yunsheng Yao*[1,2]

[1]Gansu Lanzhou Geophysics National Observation and Research Station, Lanzhou, China, [2]Lanzhou Institute of Geotechnique and Earthquake, China Earthquake Administration, Lanzhou, China, [3]Faculty of Geoscience and Environmental Engineering, Southwest Jiaotong University, Chengdu, China, [4]Institute of Surface-Earth System Science, Tianjin University, Tianjin, China

The slip rates of normal faults on the northern margin of the Ordos Block are critical for understanding the deformation of the Ordos Block and adjacent areas. In this study, we obtain the late Pleistocene slip rate of an active normal fault, the Zhuozishan West Piedmont Fault (ZWPF), in the northwestern corner of the Ordos Block. Satellite imagery interpretation and field investigations suggest that the fault displaces late Pleistocene alluvial fans and forms west-facing fault scarps. To quantify the vertical slip rate of the ZWPF, we measured the displacements along the fault scarps using differential GPS and an unmanned aerial vehicle system and dated the displaced geomorphic surfaces using optically stimulated luminescence (OSL) dating methods. The vertical slip rate of the fault is constrained to 0.1 ± 0.02 mm/a, which suggests a horizontal extension rate of 0.05 mm/a for a dip of 65°. This rate is consistent with those on similar structures in the northwestern Ordos Block. Combining this result with published slip rates along other active faults, we infer that the NW-directed extension rate across the northwestern corner of the Ordos Block is ~0.6–1.3 mm/a. This rate is comparable with the geodetic strain rate. Given the extension rate, we believe that extensional deformation is mainly concentrated on the western side of the basin.

Keywords: vertical slip rate, normal fault, Zhuozishan west piedmont fault, ordos block, slip partitioning

OPEN ACCESS

Edited by:
Chuanyou Li,
China Earthquake Administration, China

Reviewed by:
Gang Rao,
Southwest Petroleum University, China
Hu Wang,
Southwest Jiaotong University, China

***Correspondence:**
Xingwang Liu
lxw_27@163.com

Specialty section:
This article was submitted to Structural Geology and Tectonics, a section of the journal Frontiers in Earth Science

Received: *10 April 2022*
Accepted: *17 May 2022*
Published: *03 June 2022*

Citation:
Liu X, Gao Z, Shao Y and Yao Y (2022) Late Pleistocene Slip Rates on an Active Normal Fault in the Northwestern Ordos Block, China. Front. Earth Sci. 10:916905. doi: 10.3389/feart.2022.916905

INTRODUCTION

A series of basin systems have formed around the Ordos Block because of the northeastward growth of the Tibetan Plateau and the uplift of the Ordos Block since the Cenozoic; examples include the Hetao Basin to the north, the Jilantai and Yinchuan Basins to the northwest, the Shanxi Graben System to the east and the Weihe Basin to the south (**Figure 1**) (Research Group of Active Fault System around Ordos Massif, 1988). These basin systems are mainly controlled by active normal faults. The vertical slip rate of an active normal fault is an important parameter for understanding the basin evolution and regional slip partitioning (Wallace, 1987; Wesnousky, 2012; Middleton et al., 2016; Liang et al., 2018; Chevalier et al., 2020). The slip rate, together with coseismic displacement, is also used to estimate the average recurrence interval of a strong earthquake and then to estimate the seismic hazard (Wallace, 1970; Anderson, 1979; Molnar, 1979; Field, 2007). Therefore, the slip rate is one of the most important parameters in the study of an active normal fault.

The Jilantai Basin, with the Hetao Basin to the north and the Yinchuan Basin to the south (**Figure 1**), lies in the northwestern corner of the Ordos Block. The Jilantai Basin is bounded on its western side by the normal Bayanwulashan Piedmont Fault (BPF) and on its eastern side by the

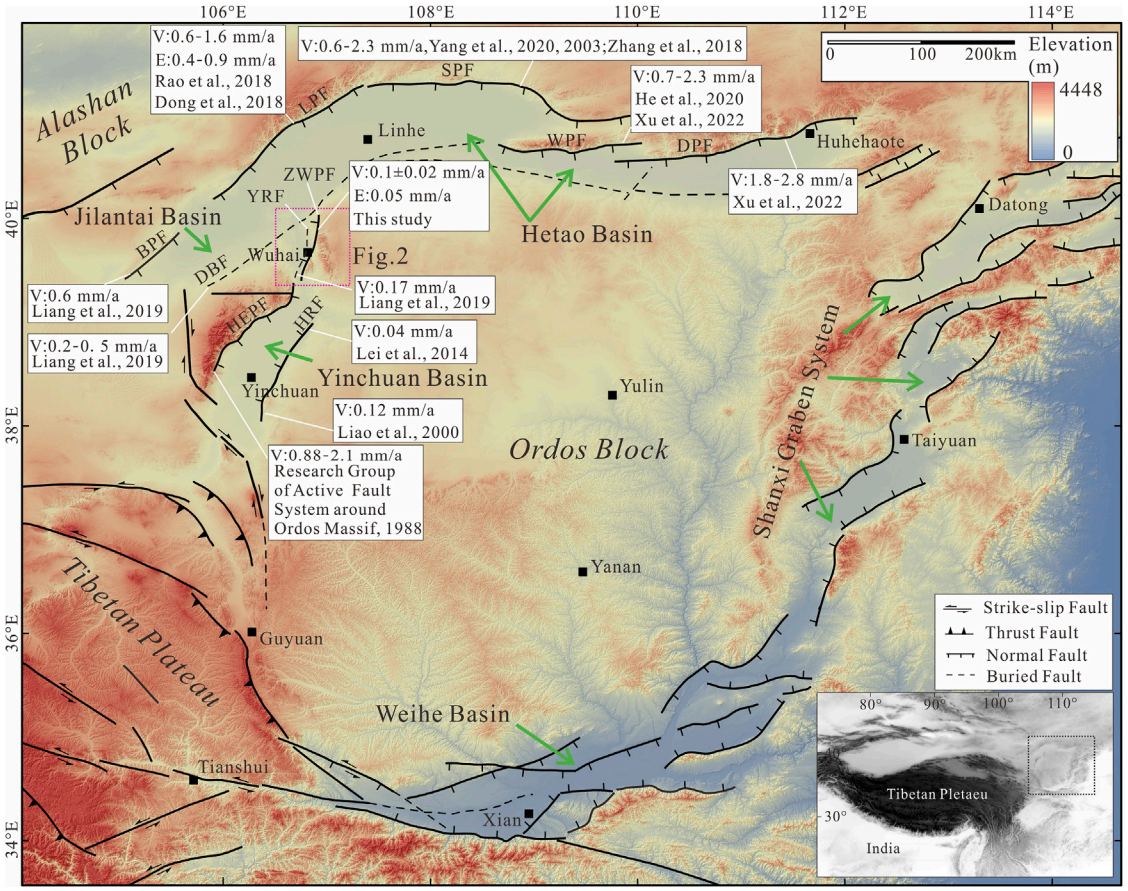

FIGURE 1 | Topographic map of the Ordos Block showing major active faults and the location of the study area. Active faults are modified from Deng (2007) and our own observations. The pink dashed rectangle shows the location of **Figure 2**. Abbreviations of names of active faults: DPF, Daqingshan Piedmont Fault; WPF, Wulashan Piedmont Fault; SPF, Seertengshan Piedmont Fault; LPF, Langshan Piedmont Fault; BPF, Bayanwulashan Piedmont Fault; DBF, Dengkou-Beijing Fault; YRF, Yellow River Fault; ZWPF, Zhuozishan West Piedmont Fault; HEPF, Helanshan East Piedmont Fault; HRF, Huanghe River Fault. V: vertical slip rate. E: extension rate.

normal Zhuozishan West Piedmont Fault (ZWPF) (**Figure 1**). For many years, the study of active faults has focused on those around the Hetao Basin and Yinchuan Basin, such as the Daqingshan Piedmont Fault (DPF) (Jiang et al., 2001; Ran et al., 2003; He et al., 2007; He and Ma, 2015), the Wulashan Piedmont Fault (WPF) (Chen, 2002; He et al., 2020), the Seertengshan Piedmont Fault (SPF) (Yang et al., 2002; Chen et al., 2003; Yang et al., 2003; Zhang et al., 2017; Rao et al., 2019), the Langshan Piedmont Fault (LPF) (Rao et al., 2016; Shen et al., 2016; Dong et al., 2018; Rao et al., 2018), and the Helanshan East Piedmont Fault (HEPF) (Deng and Liao, 1996; Lin et al., 2013; Lin et al., 2015). However, the number of studies on the ZWPF is relatively low (Liang et al., 2019).

To determine the slip rate of active faults, the displacements of landforms and corresponding ages of geomorphic surfaces are usually needed (Zhang et al., 2007; Hetzel, 2013; Liu et al., 2017, 2020; Liu et al., 2022). Using optically stimulated luminescence (OSL) dating and displacements of lacustrine layers from boreholes, Liang et al. (2019) reported a vertical slip rate of 0.5–1.0 mm/a for the ZWPF since approximately 70 ka. However, there is no limit on the geomorphic age in the study. In this contribution, to estimate the Pleistocene slip rate of the ZWPF, we use structure from motion (SfM) techniques to acquire a high-resolution digital elevation model (DEM) to determine vertical displacements, and we apply OSL dating to obtain the abandonment ages of the faulted terraces. Finally, we compare our rate with other results from the northwestern Ordos Block and discuss the roles of the ZWPF in tectonic activity and slip partitioning in the Jilantai Basin.

GEOLOGICAL BACKGROUND

The Jilantai Basin between the Gobi-Alashan and Ordos Blocks is an active faulted basin approximately 140 km long from north to south and 100 km wide from east to west (**Figure 1**). The Wuhai Basin is a subsidiary basin in the eastern of the Jilantai Basin that is approximately 100 km long from north to south and 5–15 km wide from east to west and is bounded on its eastern and western sides by the ZPWF and the Wuhushan Fault (WF) (Liang et al., 2018) (**Figure 2**). Thicknesses of Quaternary deposits within the Wuhai Basin are more than 400 m; among them, late Pleistocene

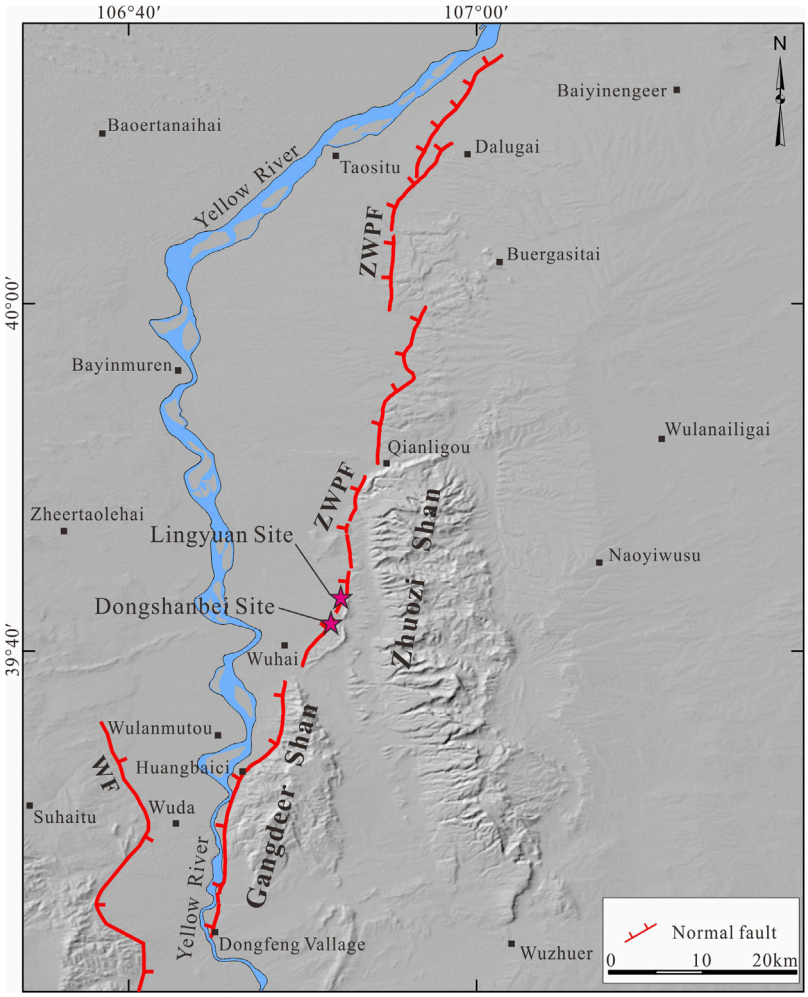

FIGURE 2 | Hill-shaded relief map showing the location of the Zhuozishan Piedmont Fault and its adjacent region. Abbreviations of names of active faults: ZPWF, Zhuozishan Piedmont Fault; WF, Wuhushan Fault.

sections are approximately 90–95 m, and the Holocene sections are approximately 10–12 m (Research Group of Active Fault System around Ordos Massif, 1998; Liang et al., 2019). The Zhuozi Shan and Gangdeer Shan are located east of the Wuhai Basin (**Figure 2**) and are mainly composed of gneiss, limestone, and shale. The crest of the Zhuozi Shan has an elevation of ~2,200 m, and the relief decreases from the crest to the Wuhai Basin at elevations of ~1,200 m. Divided by the active normal ZWPF, the ranges can be clearly separated into two regions with different landscape reliefs.

The ZWPF, which runs along the western front of the Zhuozi Shan and Gangdeer Shan with a length of 90 km, forms the eastern boundary of the Wuhai Basin (**Figure 2**). The ZWPF has experienced strong structural deformation since the Cenozoic, and its movement has changed from a thrust fault to a normal fault (Xing and Wang, 1991). The process of activity has not only created the magnificent landscape of mountains and basins but also controlled the evolution of landforms and topography since the Cenozoic. Especially since the late Quaternary, the ZWPF has faulted the piedmont alluvial fans and river terraces west of the Zhuozi Shan, forming obvious west-facing fault scarps. These well-preserved fault scarps provide an opportunity for us to study the slip rate of the fault.

METHODS

To determine the slip rate of the ZWPF, the vertical displacement should be constrained. Through satellite image interpretations, we carried out detailed field investigations and chose the appropriate study site. Based on the SfM technique (Bemis et al., 2014; Micheletti et al., 2015; Bi et al., 2017; Ai et al., 2018), we used photographs from small unmanned aerial vehicles equipped with Real-time kinematic to generate a DEM image with a resolution of centimeter accuracy for the study site. Topographic profiles perpendicular to the fault scarps were derived from the DEM image. Then, the displacement was determined from the vertical distance between the subparallel

TABLE 1 | Result of OSL analysis for the samples on the ZWPF.

Sample	Depth (m)	U-238 (Bq/kg)	Th-232 (Bq/kg)	K-40 (Bq/kg)	Dose Rate (Gy/Ka)	Equivalent dose (Gy)	OSL Age (Ka)
ZZS-OSL-01	0.7	50.9 ± 0.65	44.8 ± 2.6	512.6 ± 5.2	3.78 ± 0.10	86.85 ± 8.12	23.0 ± 3.2
ZZS-OSL-04	0.3	39.8 ± 2.05	40.2 ± 1.8	504.2 ± 8.2	3.45 ± 0.10	72.31 ± 4.59	20.9 ± 2.5
ZZS-OSL-06	0.6	45.61 ± 0.5	47.6 ± 2.6	528.2 ± 9.5	3.77 ± 0.10	95.73 ± 5.09	25.4 ± 2.9
ZZS-OSL-07	1.7	35.91 ± 4.8	36.3 ± 5.4	500.2 ± 2.5	2.99 ± 0.10	384.05 ± 23.8	128.3 ± 15.4
ZZS-OSL-08	1.5	40.55 ± 1.6	45.8 ± 2.6	564.3 ± 3.1	3.66 ± 0.10	41.80 ± 1.71	11.4 ± 1.3
ZZS-OSL-54	0.5	15 ± 1.37	27 ± 1.62	503 ± 9.51	2.88 ± 0.12	57.09 ± 1.00	19.8 ± 0.9
ZZS-OSL-55	1.6	19 ± 1.87	30 ± 1.70	566 ± 9.51	3.23 ± 0.13	41.79 ± 1.69	12.9 ± 0.7
ZZS-OSL-56	2.0	21 ± 0.75	23 ± 1.10	554 ± 9.51	2.73 ± 0.11	146.96 ± 2.91	53.9 ± 2.5
ZZS-OSL-58	0.7	20 ± 1.12	35 ± 1.58	494 ± 6.35	3.17 ± 0.13	140.43 ± 2.60	44.3 ± 1.9
ZZS-OSL-59	0.8	15 ± 3	24 ± 3	528 ± 10	3.02 ± 0.14	207.27 ± 5.53	68.7 ± 3.7
ZZS-OSL-60	0.3	11 ± 1	34 ± 3	509 ± 10	3.14 ± 0.14	72.53 ± 1.32	23.1 ± 1.1
ZZS-OSL-61	0.9	14 ± 2	31 ± 2	535 ± 10	3.16 ± 0.14	30.51 ± 0.64	9.7 ± 0.5

tread lines by fitting straight lines to both the hanging wall and footwall. At the study sites, fault outcrops are also well exposed due to stream incision and indicate that fluvial or alluvial strata have been offset by the fault. Characteristics of stratigraphic sedimentary structures and ages were used to define the activity of the fault.

OSL dating was used to constrain the age of corresponding faulted landform surfaces. Samples collected above fluvial or alluvial gravels can offer a minimum age for the time of river incision or abandonment of the landform surfaces (Pan et al., 2013; Hu et al., 2017). We hammer into the fine grain deposition with a 20 cm-long stainless-steel cube from fresh sediment sections. In the process of sample collection and packaging, we try to avoid the influence of sunlight on samples. The dating was undertaken at the Laboratory of Neotectonic Geochronology of Institute of Disaster Prevention, China Earthquake Administration, by standard procedures for Chinese loess (Forman 1991; Wang, 2006). Organic material and carbonates were removed using 30% H_2O_2 and 37% HCl under subdued red light. 4–11 μm fine-grain quartz fraction and 180–250 μm coarse-grain quartz fraction were separated after neutralization with ammonia and washing with purified water (Aitken, 1998). Then, 30% H_2SiF_6 etching was used repeatedly to remove feldspar and isolate quartz in 4–11 μm fine-grain quartz fractions. The equivalent doses of the fine-grained samples were determined using the single-aliquot regenerative-dose (SAR) dating protocol (Wang, 2006). The determination of environmental dose rate also follows the standard rules (Aitken 1998; Wang et al., 2005). The dating results are listed in **Table 1**.

RESULTS

Based on the field investigation, we select two sites (Lingyuan site and Dongshanbei site) to constrain the vertical slip rate of the ZWPF (**Figure 2**). Fault scarps of different heights are well preserved in these two sites, and we can obtain the fault slip rate in different times.

Lingyuan Site

The Lingyuan site is located in the middle segment of the ZWPF (**Figure 2**). We constructed high-resolution digital topography at this site by using the SfM technique. Then, a DEM with a resolution of 0.2 m and an associated hill-shaded relief map was acquired, which permitted us to perform a detailed analysis of tectonic landforms (**Figure 3A**). As revealed by the 0.5 m-interval contour lines, three levels of river terraces (T1-T3) can be identified based on the surface morphologies and different heights above the channel infill (**Figure 3B**). Aside from the current channel and T1 terrace, fault scarps trending approximately south-north are prominent on the hill-shaded relief map (**Figure 3A**). Moreover, an outcropping fault indicative of active deformation was also found. Field observations (**Figure 4A**) and the corresponding sketches (**Figure 4B**) indicate that a fault offsets a light-yellow fine sand layer (Unit 1), light red sandy gravel layer (Unit 2), and silty sand unit 3. The greyish-yellow loess (Unit 4) is preserved in the hanging wall. Then, the fault and sedimentary units were covered with cyan grey surface soil (Unit 5). We interpret Unit 4 as a scarp-derived deposit that usually accumulates rapidly after the creation of a fault scarp. An inverted triangular filling wedge is formed at the bottom of Unit 4. Thus, the ages of Unit 4 and Unit 3 can give limits on the timing of the most recent earthquake event. We collected and dated two OSL samples (ZZS-OSL-03 and ZZS-OSL-54) at the base of Unit 4 and Unit 3. The results show ages of 20.9 ± 2.5 ka and 19.8 ± 0.9 ka, respectively (**Table 1**). Accordingly, we think the most recent earthquake event at this locality probably occurred close to ~20 ka.

In the field, fault scarps on the T2 and T3 terraces can be clearly observed (**Figure 5A,B**). Then, we constructed two topographic profiles across the fault scraps on the DEM to constrain their heights on different terraces (**Figure 3B**). The displacement can be derived from the vertical distance between the subparallel tread lines on two fitting straight lines above and below the scarp. The heights of the fault scarp on the T2 and T3 terraces are determined to be 2.5 ± 0.2 m and 4.6 ± 0.3 m, respectively (**Figure 5C**). The vertical displacements increase with the terrace level which indicates an accumulation of fault slip.

To determine the ages of the terraces at the Lingyuan site, we collected three OSL samples from the T1, T2, and T3 terraces (**Figure 3B**). For the T1 terrace, we collected one sample from the fluvial deposit of fine-grained sand between the gravels at depths of 0.8 m, which has an age of 9.7 ± 0.5 ka (**Figure 5D**). For the T2

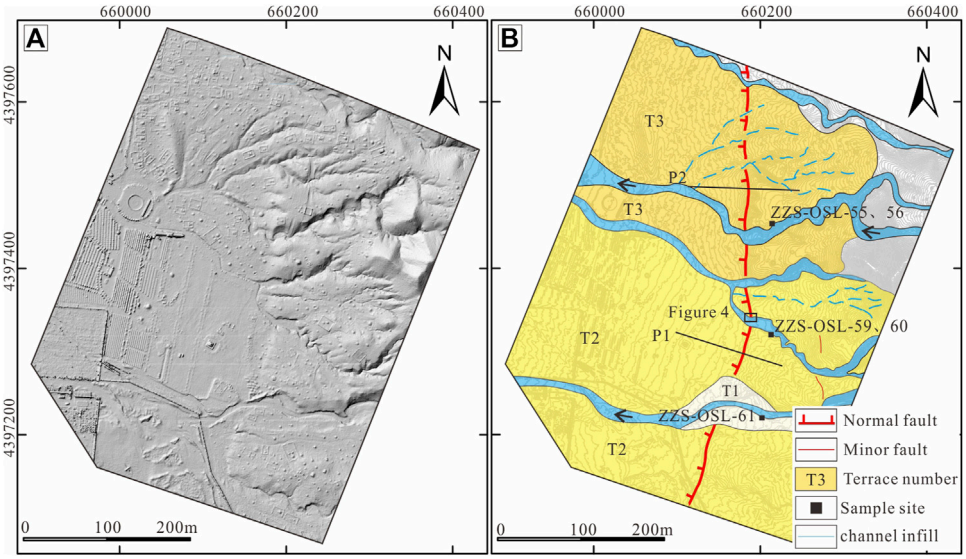

FIGURE 3 | (A) Hill-shaded relief map from high-resolution DEM data illustrating the distribution of fault scarps at the Lingyuan site **(B)** Interpreted geomorphic map with 0.5 m interval contours showing the fluvial terraces, normal fault scarps and sampling positions at the Lingyuan site. Three levels of river terraces are mapped according to their morphologic features and different heights above the channel infill.

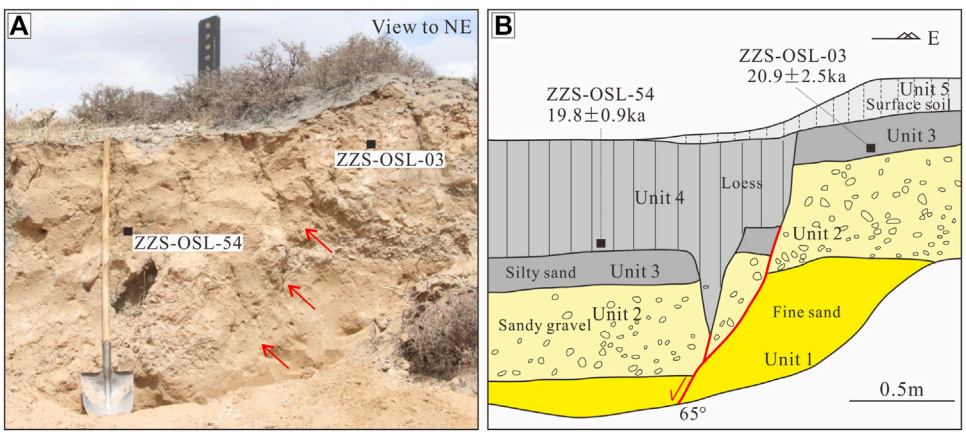

FIGURE 4 | (A) Fault outcrop underneath the scarp. The location of the fault plane is marked with red arrows **(B)** the corresponding sketch at the Lingyuan site. One major normal fault is prominent, displacing sedimentary Units 1–4. Two OSL samples (ZZS-OSL-03 and ZZS-OSL-54) collected from the faulted and covering units were dated, yielding ages of 20.9 ± 2.5 ka and 19.8 ± 0.9 ka, respectively **(Table 1)**.

terrace, two samples were collected at depths of 0.3 and 0.8 m, which are dated at 68.7 ± 3.7 ka and 23.1 ± 1.1 ka, respectively (**Figure 5E**). We think the upper sample (ZZS-OSL-59) may be mixed with underexposure material, which leads to older age. Comparing these dates with the ages of the T1 and T3 terraces, we consider 23.1 ± 1.1 ka to better represent the age of the terrace. We also collected two samples for the T3 terrace at depths of 1.6 and 2.0 m, yielding ages of 12.9 ± 0.7 ka and 53.9 ± 2.5 ka, respectively (**Figure 5F**). Considering the ages of the T1 and T2 terraces, we use 53.9 ± 2.5 ka as the age of the T3 terrace. Finally, we determine ages of 9.7 ± 0.5 ka, 23.1 ± 1.1 ka, and 53.9 ± 2.5 ka for terraces T1, T2, and T3 at the Lingyuan site, respectively.

Dongshanbei Site

The Dongshanbei site is located in eastern Wuhai city (**Figure 2**). Several nearly east-west-trending ephemeral streams rising in the Zhuozi Shan have incised into the alluvial fans and formed alluvial terraces with different heights at the mountain pass (**Figure 6A**). Four levels of alluvial terraces are identified by increasing numbers from youngest to oldest (**Figure 6B**). The terrace faces are roughly flat and dip to the west. The heights above the riverbed are approximately 2, 4.5, 9, and 15 m from the T1 to T4 terraces, respectively. The ZWPF offsets the T2, T3, and T4 terraces and forms distinct scarps facing northwest (**Figure 6B**). In the

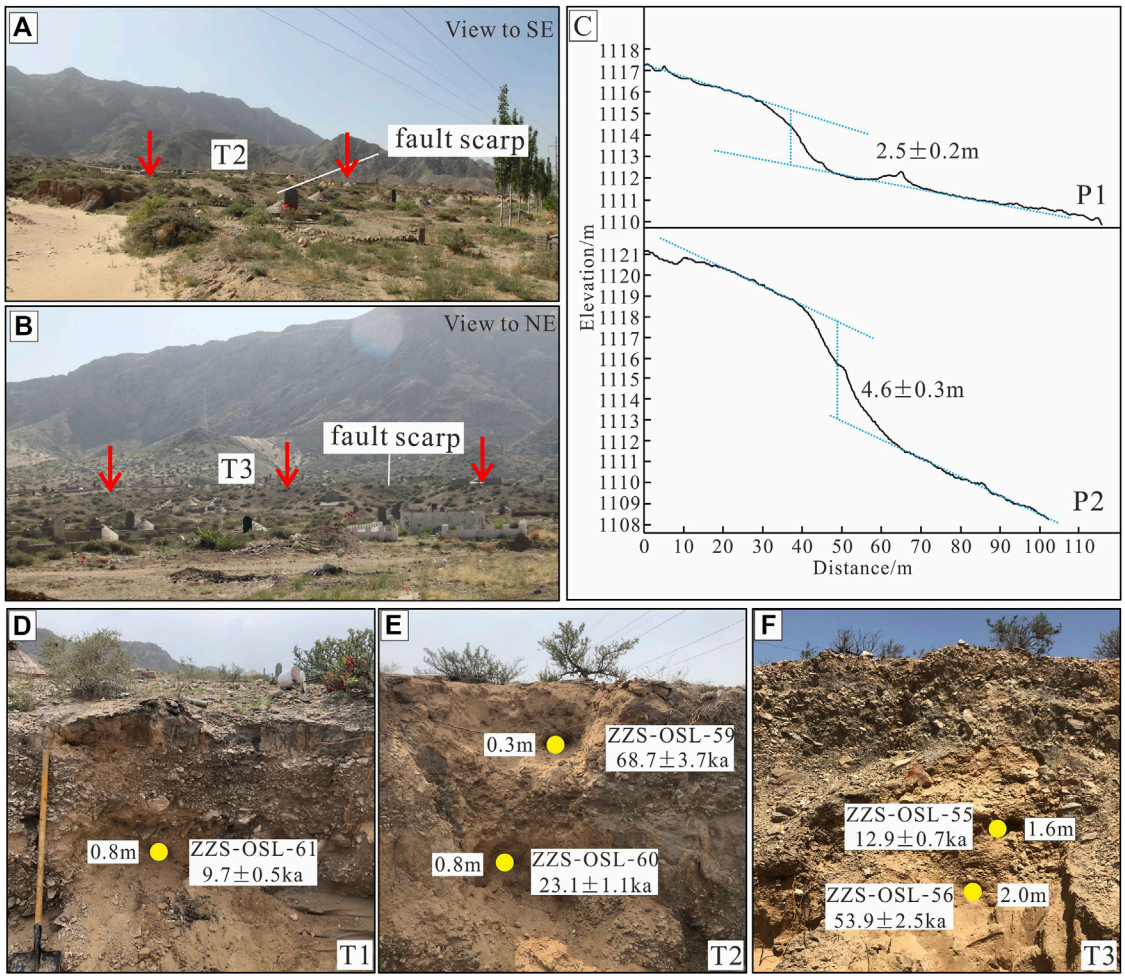

FIGURE 5 | (A) (B) Fault scarps displacing different levels of terraces observed in the field **(C)**. Topographic profiles across the fault scarps on the T2 and T3 terrace surfaces **(D) (E)**, and **(F)**. OSL sample profile and ages for T1, T2, and T3 terraces.

cliff along one stream, we find one outcrop of the fault, showing a normal component fault plane with a dip of approximately 75° (**Figure 7**). The fault displaces late Pleistocene fluvial gravels (Unit 1). Then, sandy gravel (Unit 2) has accumulated in the footwall and is overlain by loess (Unit 3). We interpret Unit 4 as a colluvial wedge that is usually accumulated rapidly after fault activity. However, it is usually difficult to obtain a suitable sample in a colluvial wedge. The age of Unit 3 can give the reference time of the most recent earthquake event. We collected and dated one OSL sample (ZZS-OSL-08) at the base of Unit 3. The results show an age of 11.4 ± 1.3 ka (**Table 1**). Accordingly, we think the most recent earthquake event at this locality probably occurred before 11.4 ± 1.3 ka. This may be the same as the latest earthquake event revealed at the Lingyuan site.

Despite the impact of erosion and human activities, fault scarps can still be distinguished on different terraces (**Figure 8A–C**). The geomorphic surface of the footwall is intact, and the hanging wall is slightly damaged. To constrain the height of the fault scarps, we carried out topographic surveys across the fault scarp with differential GPS. Three topographic profiles (P1 to P3) were obtained (**Figure 6**). By fitting straight lines to both the hanging wall and footwall, we measured the heights from P1 to P3 as 2.1 ± 0.2 m, 3.3 ± 0.1 m, and 5.4 ± 1.0 m, respectively (**Figure 8D**).

We also collected three OSL samples from the T2, T3, and T4 terraces (**Figure 6B**). For the T1 terrace, the sample was collected from the fluvial deposit of fine-grained sand between the gravels at a depth of 0.6 m, with an age of 25.4 ± 2.9 ka (**Figure 8E**). For the T2 terrace, the sample was collected at a depth of 1.7 m and was dated at 128.3 ± 15.4 ka (**Figure 8F**). We also collected one sample for the T4 terrace at 0.7 m depth, yielding an age of 44.3 ± 1.9 ka (**Figure 8G**). Comparing these dates with the ages of the T3 and T4 terraces, we believe that the date of 128.3 ± 15.4 ka cannot represent the age of the terrace. This may represent early deposition or an underexposed part of the terrace. Finally, we determine ages of 25.4 ± 2.9 ka and 44.3 ± 1.9 ka for terraces T2 and T4 at the Dongshanbei site.

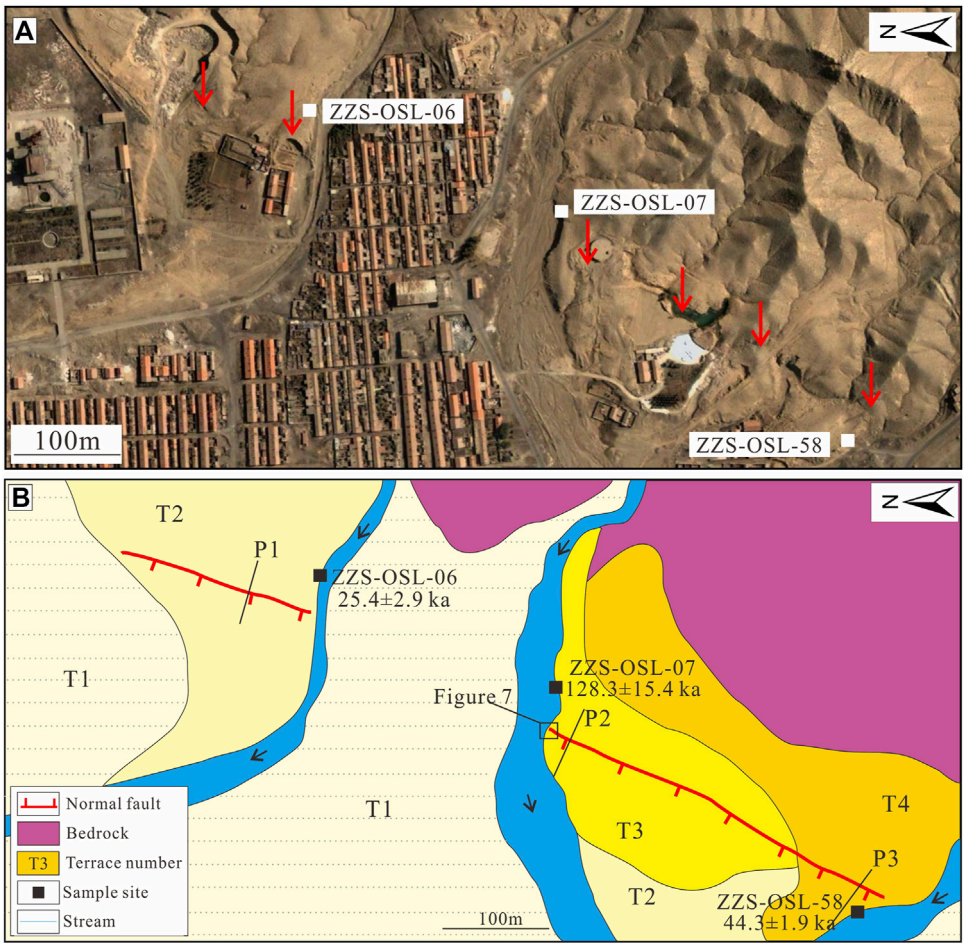

FIGURE 6 | (A) Satellite image from Google Earth. The location of fault scarps is indicated by red arrows **(B)**. Interpreted geomorphic map of the distribution of fluvial terraces, normal fault scarps and sampling positions at the Dongshanbei site. Four levels of river terraces are mapped according to their morphologic features and different heights above the channel infill.

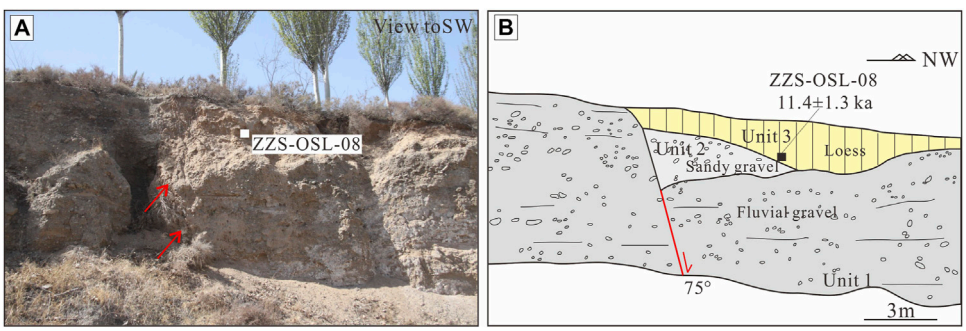

FIGURE 7 | Fault outcrop **(A)** and corresponding sketch **(B)** at the Dongshanbei site. Red arrows indicate the location of fault plane. One major normal fault is prominent, displacing sedimentary Unit 1. One OSL sample (ZZS-OSL-08) collected above the inferred colluvial wedge was dated, yielding an age of 11.4 ± 1.3 ka **(Table 1)**.

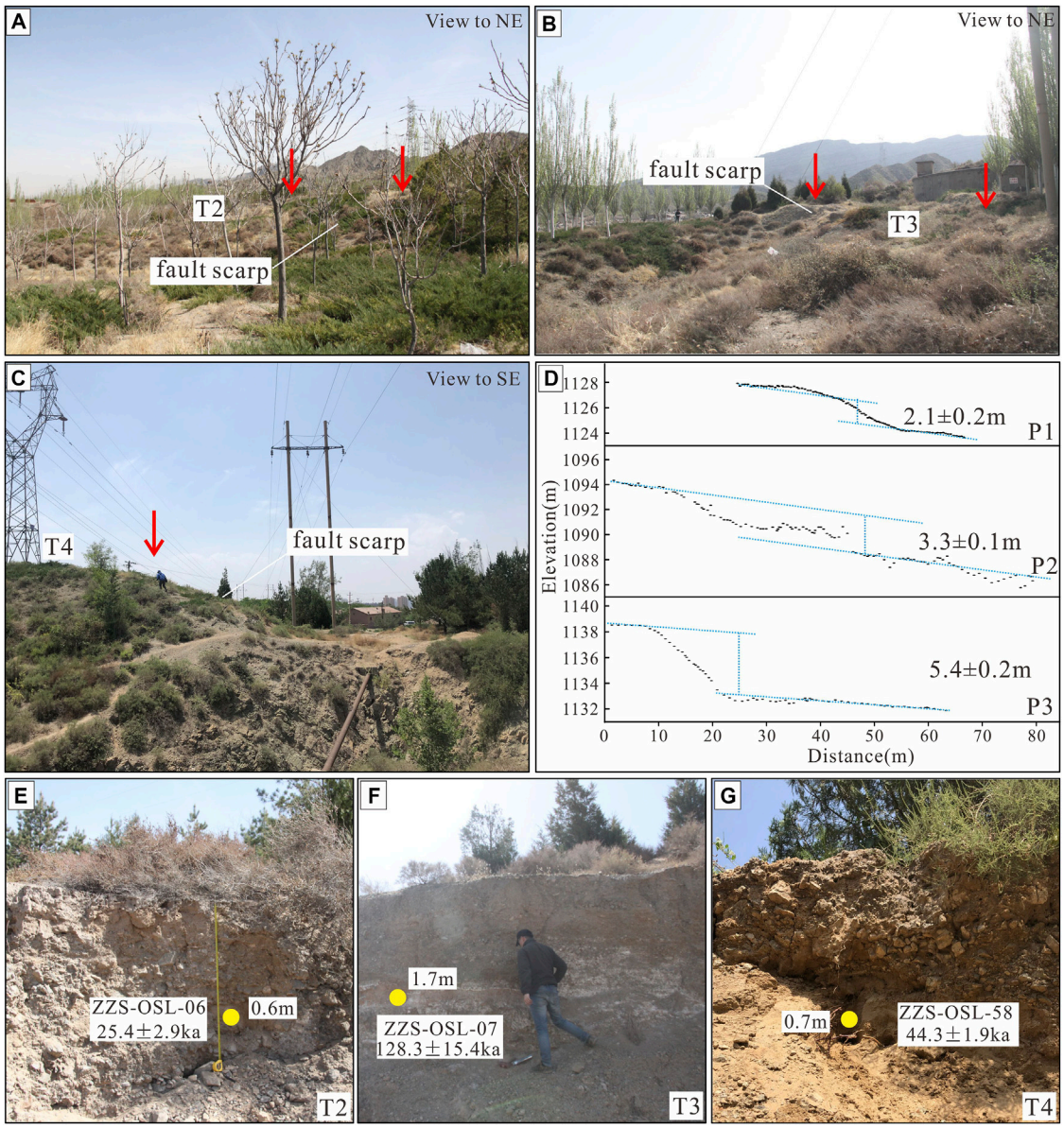

FIGURE 8 | (A) (B), and **(C)**. Fault scarps displacing different levels of terraces observed in the field **(D)**. Topographic profiles across the fault scarps on the T2, T3 and T4 terrace surfaces **(E) (F)**, and **(G)**. OSL sample profiles and ages for T2, T3, and T4 terraces.

Determination of the Slip Rate of the ZWPF

Based on the vertical offsets of the terraces and their corresponding abandonment ages, we determine the vertical component of the slip rate. The uncertainty comes mainly from uncertainties in the ages and the vertical offsets. At the Lingyuan site, an average slip rate of 0.1 ± 0.02 mm/a is determined using vertical displacements (2.5 ± 0.2 m and 4.6 ± 0.3 m) and corresponding ages (23.1 ± 1.1 ka and 53.9 ± 2.5 ka) (**Figure 9A**). At the Dongshanbei site, we derive an average slip rate of 0.1 ± 0.02 mm/a by using vertical displacements (2.1 ± 0.2 m and 5.4 ± 0.2 m) and corresponding ages (25.4 ± 2.9 ka and 44.3 ± 1.9 ka) (**Figure 9B**). The two research points are close to each other and show the same vertical slip rate. This also reflects that our results are reliable. Trenches and natural outcrops reveal that the range of fault dips is ~50°–80° to the west (Zhang, 2014; Liang et al., 2019; Gao, 2020). With an average dip of ~65° and a vertical slip rate of 0.1 ± 0.02 mm/a, the extension rate is estimated to be ~0.05 mm/a.

DISCUSSION

Comparison With Other Active Faults in the Close Region

The active faults in the northwestern Ordos Block are in a similar tectonic stress field. Therefore, the slip rate of faults should be comparable or regular. There are three basins in the northwestern Ordos Block, the Yinchuan Basin, the Jilantai Basin, and the

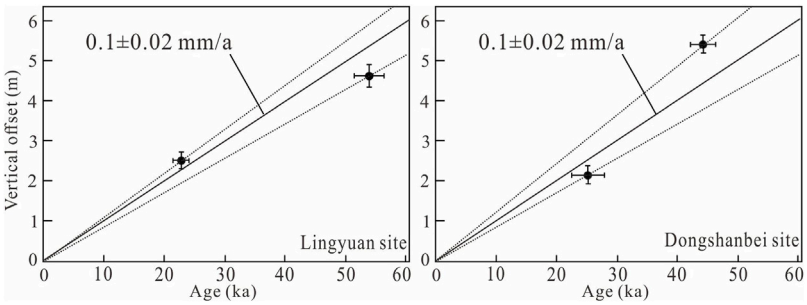

FIGURE 9 | Average vertical slip rates on the ZWPF, which are estimated from vertical offsets recorded by terraces T2 and T3 at the Lingyuan site and T2 and T4 at the Dongshanbei site and their corresponding abandonment ages.

Hetao Basin (**Figure 1**). These basins are mainly controlled by active faults on both sides.

The Yinchuan Basin is bounded on its western side by the normal HEPF and on its eastern side by the normal YRF. For the HEPF, the vertical slip rate has a range of 0.88–2.1 mm/a (Research Group of Active Fault System around Ordos Massif, 1988). The southern segment of the YRF faults surface landform and forms fault scarps. Based on fault scarp measurements and thermoluminescence dating, the vertical slip rate was determined to be 0.12 mm/a (Liao et al., 2000). The northern segment of the YRF is buried. According to borehole displacement measurements and OSL dating, an average vertical slip rate of 0.04 mm/a is obtained (Lei et al., 2014). The normal Bayanwulashan Piedmont Fault (BPF) is the western boundary of the Jilantai Basin. Its vertical slip rate is estimated to be approximately 0.6 mm/a since the late Pleistocene (Liang et al., 2019). At the eastern boundary of the Jilantai Basin and to the west of ZWPF, there is also a buried fault called the Yellow River Fault (YRF). Liang et al. (2018) obtained a vertical slip rate of 0.17 mm/a for the fault by using drill cores and Quaternary dating methods.

The Langshan Piedmont Fault (LPF), Seertengshan Piedmont Fault (SPF), Wulashan Piedmont Fault (WPF), and the Daqingshan Piedmont Fault (DPF) are the western and northern boundary faults of the Hetao Basin. The LPF is located on the northwestern margin of the Hetao Basin. Previous studies have suggested that the vertical slip rate of the LPF is ~0.5–2.2 mm/a (Research Group of Active Fault System around Ordos Massif, 1988; Deng et al., 1999). According to the coseismic displacement and recurrence interval, the vertical slip rate of the LPF is limited to ~0.6–1.6 mm/a (Dong et al., 2018; Rao et al., 2018). For the SPF, many results suggested that the vertical slip rate of the fault is ~0.6–2.3 mm/a (Yang et al., 2002, 2003; Zhang et al., 2017). He et al. (2020) and Xu et al. (2022) reported slip rates of ~0.7–2.3 mm/a for the WPF since the late Pleistocene. For the DPF, the latest results show that the Holocene vertical slip rate of the fault is ~1.8–2.8 mm/a (Xu et al., 2022). However, the activity of the faults on the southern boundary of the Hetao Basin is low, and quantitative research is lacking.

From the comparison of fault slip rates in the northwestern Ordos Block, we found that the slip rates of active faults on the northern and western boundaries of the basins are high, with an average of more than 1 mm/a, and the values in the southern and eastern boundaries of the basins are low and maybe less than 0.2 mm/a. We infer that this may be related to the subsurface structural architecture. Asymmetric half-graben structures have been formed in these basins, and the subsidence centers are close to the northern and western sides (Research Group of Active Fault System around Ordos Massif, 1988; Lei, 2106; Liang et al., 2018; Rao et al., 2018).

Implications for slip partitioning in the northwestern corner of Ordos Block

The Ordos Block is characterized by counter-clockwise rotation because of the expansion of the Tibetan Plateau and the subduction of the Pacific Plate (Zhang et al., 2002, 2005; Liang et al., 2018). The eastern and western sides of the Ordos Block are the Yinchuan-Jilantai Basin and Shanxi Graben System controlled by dextral normal faults. The southern and northern sides of the Ordos Block are the Weihe Basin and Hetao Basin controlled by sinistral normal faults (Zhang et al., 2002, 2005). The Jilantai Basin and the western part of the Hetao Basin lie in the northwestern corner of the Ordos Block and should be characterized by both extensional and dextral movement. The latest GPS data also reflect these features (Zhao et al., 2017). The extension and dextral slip rates across the northwestern corner of the Ordos Block in the NW direction were deduced to be 1.6 ± 0.4 mm/a and 0.8 ± 0.7 mm/a from GPS velocities, respectively (Zhao et al., 2017). These rates are distributed on a series of active faults across the region.

The extension rate associated with active normal faulting can be assessed in combination with near-surface exposed fault dips (Zhang et al., 1998; Personius et al., 2017). The GPS profile crosses mainly the LPF, the ZWPF, and the Yellow River Fault. The vertical slip rate of the LPF is determined to be ~0.6–1.6 mm/a (Dong et al., 2018; Rao et al., 2018), with a dip of ~60° (Research Group of Active Fault System around Ordos Massif 1988; Rao et al., 2018) and the extension rate is estimated to be ~0.4–0.9 mm/a. In this study, the vertical slip rate of the ZWPF is determined to be 0.1 ± 0.02 mm/a. In the eastern part of the basin, the vertical slip rate of the buried Yellow River fault was determined to be 0.17 mm/a (Liang et al.,

2018). For another buried fault within the basin, namely, the Dengkou-Benjing Fault (DBF), the vertical slip rate is inferred to be 0.2–0.5 mm/a (Liang et al., 2019). The total vertical slip rate in the eastern part of the basin would be ~0.5–0.8 mm/a. If these faults have dips of ~65° similar to the ZWPF, the extension rate would be 0.2–0.4 mm/a. Therefore, the total extension rate across the northwestern corner of the Ordos Block would be ~0.6–1.3 mm/a. This value seems lower than the GPS data (Zhao et al., 2017). If we consider a decrease in fault dip, for example, fault planes flattening with depth and developing listric geometry, the results would become comparable with the GPS data. Comparing the extension rates, we infer that the main extensional deformation occurs on the western side of the basin.

Meanwhile, GPS data also reflect dextral shearing across the northwestern corner of the Ordos Block (Zhao et al., 2017). Unfortunately, we did not find evidence of dextral slip along the ZWPF. Similarly, the LPF on the western side of the basin was demonstrated to show almost pure normal slip (Dong et al., 2018; Rao et al., 2018). The active faults in the northern Ordos Block also do not display the characteristics of sinistral slip reflected by GPS (Zhang et al., 2017; He et al., 2019; Rao et al., 2019; He et al., 2020, Rao et al., 2020). According to the focal mechanism solution of two earthquakes, Rao et al. (2018) inferred that dextral slip movements mostly occur on buried faults within the basin. Normal-faulting earthquakes are mainly concentrated on the margin of the basin (Wen, 2014; Liang et al., 2019). The same situation can also be found in the Yinchuan Basin (Middleton, et al., 2016; Liang et al., 2019). If this is a common phenomenon, the result would help us to better understand the slip characteristics of active faults in other basins around the Ordos Block.

CONCLUSION

The ZWPF, along the western margin of the Zhuozi Shan, forms the eastern boundary of the Jilantai Basin, has grown by normal faulting, and was active during the Pleistocene. The latest earthquake event was dated to ~20 ka. Satellite image interpretations and field investigations show that the fault offsets late Quaternary terraces and alluvial fans and forms permanent west-facing fault scarps. Based on OSL dating, we obtain the abandonment ages of the faulted terraces. Combining the ages and fault scarp heights obtained from the high-resolution DEM and differential GPS measurements, the vertical slip rate of the ZWPF is determined to be 0.1 ± 0.02 mm/a since the Pleistocene, which suggests an extension rate of 0.05 mm/a with a dip of ~65°. Combining these values with other results, we infer that the NW-directed extension rate across the Jilantai Basin will be ~0.6–1.3 mm/a. The extensional deformation mainly occurred on the western side of the basin.

DATA AVAILABILITY STATEMENT

The original contributions presented in the study are included in the article/supplementary material, further inquiries can be directed to the corresponding author.

AUTHOR CONTRIBUTIONS

XL carried out field work, drew the figures, and wrote the manuscript. GZ, YS, and YY performed the fieldwork, sampling, aerial photogrammetry, and differential GPS measurements. All authors discussed the results and contributed to the manuscript.

FUNDING

This work was supported by the National Key Research and Development Program of China (2017YFC1500100) and the Innovation Team Project of Earthquake Administration of Gansu Province (2019TD0101).

ACKNOWLEDGMENTS

We are grateful to Daoyang Yuan, Wenjun Zheng, Qiyun Lei, and Chuanyong Wu for their discussions and suggestions in the field regarding our preliminary results. We greatly thank the reviewers and editors for their constructive and detailed comments to improve the manuscript.

REFERENCES

Ai, M., Bi, H., Zheng, W., Yin, J., Yuan, D., Ren, Z., et al. (2018). Using Unmanned Aerial Vehicle Photogrammetry Technology to Obtain Quantitative Parameters of Active Tectonics. *Seismol. Geol.* 40, 1276–1293.

Aitken, M. J. (1998). *An Introduction to Optical Dating: The Dating of Quaternary Sediments by the Use of Photon-Stimulated Luminescence*. Oxford: Oxford University Press.

Anderson, J. G. (1979). Estimating the Seismicity from Geological Structure for Seismic-Risk Studies. *Bull. Seismol. Soc. Am.* 69, 135–158. doi:10.1785/BSSA0690010135

Bemis, S. P., Micklethwaite, S., Turner, D., James, M. R., Akciz, S., Thiele, S. T., et al. (2014). Ground-based and UAV-Based Photogrammetry: A Multi-Scale, High-Resolution Mapping Tool for Structural Geology and Paleoseismology. *J. Struct. Geol.* 69, 163–178. doi:10.1016/j.jsg.2014.10.007

Bi, H., Zheng, W., Ren, Z., Zeng, J., and Yu, J. (2017). Using an Unmanned Aerial Vehicle for Topography Mapping of the Fault Zone Based on Structure from Motion Photogrammetry. *Int. J. Remote Sens.* 38, 2495–2510. doi:10.1080/01431161.2016.1249308

Chen, L., Ran, Y., and Chang, Z. (2003). Characteristics of Late Quaternary Faulting and Paleoseismic Events on the East of Delingshan Segment of the Sertengshan Piedmont Fault. *Seismol. Geol.* 25, 555–565.

Chen, L. (2002). *Paleoearthquakes, the Law of Strong Earthquake Recurrence and Potential Sites for the Occurrence of Future Strong Earthquakes in the Hetao Fault-Depression Zone*. Beijing, China: Institute of Geology, China Earthquake Administration. Master Thesis.

Chevalier, M. L., Tapponnier, P., Woerd, J., Leloup, P. H., Wang, S., Pan, J., et al. (2020). Late Quaternary Extension Rates across the Northern Half of the Yadong-Gulu Rift: Implication for East-West Extension in Southern Tibet. *J. Geophys. Res. Solid Earth* 125, e2019JB019106. doi:10.1029/2019JB019106

Deng, Q., and Liao, Y. (1996). Paleoseismology along the Range-Front Fault of Helan Mountains, North Central China. *J. Geophys. Res.* 101, 5873–5893. doi:10.1029/95jb01814

Deng, Y., Wang, J., Harvey, J., Yang, G., and Ren, D. (1999). Discussion on Cenozoic Tectonics and Dynamics of Ordos Block. *J. Geomech.* 186, 13–23. doi:10.1023/a:1005186016971

Deng, Q. (2007). *Active Tectonics Map of China*. Beijing: Seismological Press.

Dong, S., Zhang, P., Zheng, W., Yu, Z., Lei, Q., Yang, H., et al. (2018). Paleoseismic Observations along the Langshan Range-Front Fault, Hetao Basin, China: Tectonic and Seismic Implications. *Tectonophysics* 730, 63–80. doi:10.1016/j.tecto.2018.02.012

Field, E. H. (2007). A Summary of Previous Working Groups on California Earthquake Probabilities. *Bull. Seismol. Soc. Am.* 97, 1033–1053. doi:10.1785/0120060048

Forman, S. L. (1991). Late Pleistocene Chronology of Loess Deposition Near Luochuan, China. *Quat. Res.* 36, 19–28. doi:10.1016/0033-5894(91)90014-V

Gao, Z. (2020). *Late Quaternary Activity Characteristics and Risk Analysis of Large Earthquakes of the Zhuozishan West Piedmont Fault*. Lanzhou, China: Lanzhou Institute of Seismology, China Earthquake Administration. Master Thesis.

He, C., Rao, G., Yang, R., Hu, J., Yao, Q., and Yang, C. (2019). Divide Migration in Response to Asymmetric Uplift: Insights From the Wula Shan Horst, North China. *Geomorphology* 339, 44–57. doi:10.1016/j.geomorph.2019.04.024

He, Z., and Ma, B. (2015). Holocene Paleoearthquakes of the Daqingshan Fault Detected from Knickpoint Identification and Alluvial Soil Profile. *J. Asian Earth Sci.* 98, 261–271. doi:10.1016/j.jseaes.2014.11.025

He, Z., Ma, B., and Lu, H. (2007). Segmentation of Active Fault Zones and Potential Focal Areas in the Piedmont of Daqing Mountain. *Seismol. Geol.* 29, 765–775.

He, Z., Ma, B., Hao, Y., Zhao, J., and Wang, J. (2020). Surface Rupture Geomorphology and Vertical Slip Rates Constrained by Terraces along the Wulashan Piedmont Fault in the Hetao Basin, China. *Geomorphology* 358, 107116. doi:10.1016/j.geomorph.2020.107116

Hetzel, R. (2013). Active Faulting, Mountain Growth, and Erosion at the Margins of the Tibetan Plateau Constrained by In Situ-produced Cosmogenic Nuclides. *Tectonophysics* 582, 1–24. doi:10.1016/j.tecto.2012.10.027

Hu, X., Pan, B., Fan, Y., Wang, J., Hu, Z., Cao, B., et al. (2017). Folded Fluvial Terraces in a Young, Actively Deforming Intramontane Basin between the Yumu Shan and the Qilian Shan Mountains, NE Tibet. *Lithosphere* 9, L614.1–560. doi:10.1130/L614.1

Jiang, W., Xiao, Z., Wang, H., and Gong, F. (2001). Segmentation Character of Seismic Surface Ruptures of the Piedmont Active Fault of MT. Daqingshan, Inner Monglia. *Seismol. Geol.* 23, 24–34.

Lei, Q., Chai, C., Zheng, W., Du, P., Xie, X., Wang, Y., et al. (2014). Active and Slip Rate in the Northern Section of the Yellow River Fault by Drilling. *Seismol. Geol.* 36, 464–477.

Lei, Q. Y. (2016). *The Extension of the Arc Tectonic Belt in the Northeastern Margin of the Tibet Plateau and the Evolution of the Yinchuan Basin in the Western Margin of the North China*. Beijing, China: Institute of Geology, China Earthquake Administration. Doctoral Thesis.

Liang, K., Sun, C., Ma, B., Tian, Q., Li, D., Li, D., et al. (2018). Investigation of the Yellow River Buried Fault in the Wuhai Basin, Northwestern Ordos Block, China, Using Deep/shallow Seismic Reflection and Drilling Techniques. *J. Asian Earth Sci.* 163, 54–69. doi:10.1016/j.jseaes.2018.05.025

Liang, K., Ma, B., Li, D., Tian, Q., Sun, C., He, Z., et al. (2019). Quaternary Activity of the Zhuozishan West Piedmont Fault Provides Insight into the Structural Development of the Wuhai Basin and Northwestern Ordos Block, China. *Tectonophysics* 754, 56–72. doi:10.1016/j.tecto.2019.02.004

Liao, Y., Chai, C., Zheng, W., and Xu, W. (2000). The Active Features and Slip Rate of Lingwu Faults in Late Quaternary. *Earthq. Res. China* 16, 158–165.

Lin, A., Rao, G., Hu, J., and Gong, W. (2013). Reevaluation of the Offset of the Great Wall Associated with the Ca. M 8.0 Pingluo Earthquake of 1739, Yinchuan Graben, China. *J. Seismol.* 17, 1281–1294. doi:10.1007/s10950-013-9391-2

Lin, A., Hu, J., and Gong, W. (2015). Active Normal Faulting and the Seismogenic Fault of the 1739 M ~8.0 Pingluo Earthquake in the Intracontinental Yinchuan Graben, China. *J. Asian Earth Sci.* 114, 155–173. doi:10.1016/j.jseaes.2015.04.036

Liu, X.-W., Yuan, D.-Y., and Su, Q. (2017). Late Pleistocene Slip Rate of the Northern Qilian Shan Frontal Thrust, Western Hexi Corridor, China. *Terra nova.*. 29, 238–244. doi:10.1111/ter.12270

Liu, X., Yuan, D., Su, Q., and Zhang, B. (2020). Late Quaternary Tectonic Activity and Slip Rates of Active Faults in the Western Hexi Corridor, NW China. *J. Earth Sci.* 31, 968–977. doi:10.1007/s12583-020-1287-9

Liu, J., Ren, Z., Zhang, H., Li, C., Zhang, Z., Zheng, W., et al. (2022). Slip Rates along the Laohushan Fault and Spatial Variation in Slip Rate along the Haiyuan Fault Zone. *Tectonics* 41, e2021TC006992. doi:10.1029/2021TC006992

Micheletti, N., Chandler, J. H., and Lane, S. N. (2015). Investigating the Geomorphological Potential of Freely Available and Accessible Structure-From-Motion Photogrammetry Using a Smartphone. *Earth Surf. Process. Landforms* 40, 473–486. doi:10.1002/esp.3648

Middleton, T. A., Walker, R. T., Rood, D. H., Rhodes, E. J., Parsons, B., Lei, Q., et al. (2016). The Tectonics of the Western Ordos Plateau, Ningxia, China: Slip Rates on the Luoshan and East Helanshan Faults. *Tectonics* 35, 2754–2777. doi:10.1002/2016TC004230

Molnar, P. (1979). Earthquake Recurrence Intervals and Plate Tectonics. *Bull. Seism. Soc. Am.* 69, 115–133. doi:10.1007/BF0231005110.1785/bssa0690010115

Pan, B., Hu, X., Gao, H., Hu, Z., Cao, B., Geng, H., et al. (2013). Late Quaternary River Incision Rates and Rock Uplift Pattern of the Eastern Qilian Shan Mountain, China. *Geomorphology* 184, 84–97. doi:10.1016/j.geomorph.2012.11.020

Personius, S. F., Briggs, R. W., Maharrey, J. Z., Angster, S. J., and Mahan, S. A. (2017). A Paleoseismic Transect across the Northwestern Basin and Range Province, Northwestern Nevada and Northeastern California, USA. *USAGeosphere* 13, 782–810. doi:10.1130/GES01380.1

Ran, Y., Zhang, P., and Chen, L. (2003). Research on the Completeness of Paleoseismic Activity History since Late Quaternary along the Daqingshan Piedmont Fault in Hetao Depression Zone, North China. *Earth Sci. Front.* 10, 207–216.

Rao, G., Chen, P., Hu, J., Yu, Y., and Qiu, J. (2016). Timing of Holocene Paleo-Earthquakes along the Langshan Piedmont Fault in the Western Hetao Graben, North China: Implications for Seismic Risk. *Tectonophysics* 677-678, 115–124. doi:10.1016/j.tecto.2016.03.035

Rao, G., He, C., Cheng, Y., Yu, Y., Hu, J., Chen, P., et al. (2018). Active Normal Faulting along the Langshan Piedmont Fault, North China: Implications for Slip Partitioning in the Western Hetao Graben. *J. Geol.* 126, 99–118. doi:10.1086/694748

Rao, G., He, C., Chen, P., Wu, Z., Hu, J., and Yao, Q. (2019). Active Normal Faulting along the Seerteng Shan, North China: Geometry and Kinematics. *J. Asian Earth Sci.* 184, 103976. doi:10.1016/j.jseaes.2019.103976

Rao, G., He, C., Chen, H., Yang, X., Shi, X., Chen, P., et al. (2020). Use of Small Uunmanned Aerial Vehicle (sUAV)-Acquired Topography for Identifying and Characterizing Active Normal Faults Along the Seerteng Shan, North China. *Geomorphology* 359. doi:10.1016/j.geomorph.2020.107168

Research Group of Active Fault System around Ordos Massif (1988). *Active Fault System Around Ordos Massif*. Beijing, China: Seismological Press.

Shen, X.-m., Li, D.-w., Tian, Y.-t., Lv, Y.-w., Li, D.-w., and Li, Y.-f. (2016). Late Pleistocene - Holocene Slip History of the Langshan-Seertengshan Piedmont Fault (Inner Mongolia, Northern China) from Cosmogenic 10Be Dating on a Bedrock Fault Scarp. *J. Mt. Sci.* 13, 882–890. doi:10.1007/s11629-015-3717-1

Wallace, R. E. (1970). Earthquake Recurrence Intervals on the San Andreas Fault. *Geol. Soc. Am. Bull.* 81, 2875–2890. doi:10.1130/0016-7606(1970)81[2875:eriots]2.0.co;2

Wallace, R. E. (1987). Grouping and Migration of Surface Faulting and Variations in Slip Rates on Faults in the Great Basin Province. *Bull. Seismol. Soc. Am.* 77, 868–876. doi:10.1016/0040-1951(87)90059-X

Wang, X., Lu, Y., and Li, X. (2005). Luminescence Dating of Fine-grained Quartz in Chinese Loess-Simplified Multiple Aliquot Regenerative-Dose (MAR) Protocol. *Seismol. Geol.* 27, 615–623.

Wang, X., Lu, Y., and Zhao, H. (2006). On the Performances of the Single-Aliquot Regenerative-Dose (SAR) Protocol for Chinese Loess: Fine Quartz and Polymineral Grains. *Radiat. Meas.* 41, 1–8. doi:10.1016/j.radmeas.2005.02.010

Wen, X. (2014). Structures of Source Regions of the 1979 Ms 6.0 Wuyuan Earthquake and the 1996 Ms Baotou Earthquake in Inner Mongolia, China. *Seismol. Geol.* 36, 586–597.

Wesnousky, S. G. (2012). Earthquakes, Quaternary Faults, and Seismic Hazard in California. *J. Geophys. Res.* 91, 12587–12631. doi:10.1029/JB091iB12p12587

Xing, C., and Wang, W. (1991). Zhuozishan Fault Zone and its Neoactive Characteristics. *J. Northwest. Seismol.* 13, 86–88.

Xu, D., He, Z., Ma, B., Long, J., Zhang, H., and Liang, K. (2022). Vertical Slip Rates of Normal Faults Constrained by Both Fault Walls: A Case Study of the Hetao Fault System in Northern China. *Front. Earth Sci.* 10, 816922. doi:10.3389/feart.2022.816922

Yang, X., Ran, Y., Hu, B., and Guo, W. (2002). Active Fault and Paleoearthquakes of the Piedmont Fault (Wuju-Mengkou-Dongfeng Village) for Seerteng Mountains, Inner Mongolia. *Earthq. Res. China* 18, 127–140.

Yang, X., Ran, Y., Hu, B., and Guo, W. (2003). Paleoseismic Activity on Wujiahe Segment of Sertengshan Piedmont Fault, Inner Mongolia. *Acta Seismol. Sin.* 25, 62–71.

Zhang, Y. Q., Mercier, J. L., and Vergély, P. (1998). Extension in the Graben Systems Around the Ordos (China), and its Contribution to the Extrusion Tectonics of South China with Respect to Gobi-Mongolia. *Tectonophysics* 285, 41–75. doi:10.1016/s0040-1951(97)00170-4

Zhang, P., Wang, Q., and Ma, Z. (2002). GPS Velocity Field and Active Crustal Blocks of Contemporary Tectonic Deformation in Continental China. *Earth Sci. Front.* 9, 430–441.

Zhang, P., Gan, W., Shen, Z., and Wang, M. (2005). A Coupling Model of Rigid-Block Movement and Continuous Deformation: Patterns of the Present-Day Deformation of Chinas Continent and its Vicinity. *Acta Seismol. Sin.* 79, 748–756.

Zhang, P.-Z., Molnar, P., and Xu, X. (2007). Late Quaternary and Present-Day Rates of Slip along the Altyn Tagh Fault, Northern Margin of the Tibetan Plateau. *Tectonics* 26, TC5010. doi:10.1029/2006tc002014

Zhang, H., He, Z., Ma, B., Long, J., Liang, K., and Wang, J. (2017). The Vertical Slip Rate of the Sertengshan Piedmont Fault, Inner Mongolia, China. *J. Asian Earth Sci.* 143, 95–108. doi:10.1016/j.jseaes.2017.04.014

Zhang, Y. (2014). *Late Quaternary Activity of the Zhuozishan Western Piedmont Fault*. Beijing, China: Institute of Crustal Dynamics, China Earthquake Administration. Master Thesis.

Zhao, B., Zhang, C., Wang, D., Huang, Y., Tan, K., Du, R., et al. (2017). Contemporary Kinematics of the Ordos Block, North China and its Adjacent Rift Systems Constrained by Dense GPS Observations. *J. Asian Earth Sci.* 135, 257–267. doi:10.1016/j.jseaes.2016.12.045

Conflict of Interest: The authors declare that the research was conducted in the absence of any commercial or financial relationships that could be construed as a potential conflict of interest.

Publisher's Note: All claims expressed in this article are solely those of the authors and do not necessarily represent those of their affiliated organizations, or those of the publisher, the editors and the reviewers. Any product that may be evaluated in this article, or claim that may be made by its manufacturer, is not guaranteed or endorsed by the publisher.